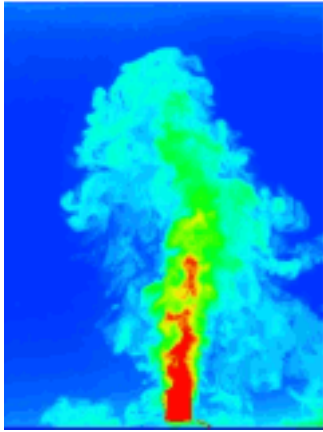


This article was downloaded by: [Kungliga Tekniska Hogskola]

On: 24 October 2012, At: 04:17

Publisher: Taylor & Francis

Informa Ltd Registered in England and Wales Registered Number: 1072954 Registered office: Mortimer House, 37-41 Mortimer Street, London W1T 3JH, UK



Journal of Turbulence

Publication details, including instructions for authors and subscription information:

<http://www.tandfonline.com/loi/tjot20>

Nonlinear receptivity to oblique vortical modes in flow past an elliptic leading edge

Lars-Uve Schrader^a, Catherine Mavriplis^a, Luca Brandt^b & Dan S. Henningson^b

^a Department of Mechanical Engineering, University of Ottawa, K1N 6N5, Ottawa, Canada

^b Linné Flow Centre, KTH Mechanics, SE-100 44, Stockholm, Sweden

Version of record first published: 06 Jul 2012.

To cite this article: Lars-Uve Schrader, Catherine Mavriplis, Luca Brandt & Dan S. Henningson (2012): Nonlinear receptivity to oblique vortical modes in flow past an elliptic leading edge, *Journal of Turbulence*, 13, N25

To link to this article: <http://dx.doi.org/10.1080/14685248.2012.695076>

PLEASE SCROLL DOWN FOR ARTICLE

Full terms and conditions of use: <http://www.tandfonline.com/page/terms-and-conditions>

This article may be used for research, teaching, and private study purposes. Any substantial or systematic reproduction, redistribution, reselling, loan, sub-licensing, systematic supply, or distribution in any form to anyone is expressly forbidden.

The publisher does not give any warranty express or implied or make any representation that the contents will be complete or accurate or up to date. The accuracy of any instructions, formulae, and drug doses should be independently verified with primary sources. The publisher shall not be liable for any loss, actions, claims, proceedings, demand, or costs or damages whatsoever or howsoever caused arising directly or indirectly in connection with or arising out of the use of this material.

Nonlinear receptivity to oblique vortical modes in flow past an elliptic leading edge

Lars-Uve Schrader^{a*}, Catherine Mavriplis^a, Luca Brandt^b and Dan S. Henningson^b

^aDepartment of Mechanical Engineering, University of Ottawa, Ottawa, Canada K1N 6N5;

^bLinné Flow Centre, KTH Mechanics, SE-100 44 Stockholm, Sweden

(Received 20 October 2011; final version received 7 May 2012)

Nonlinear boundary-layer receptivity to pairs of unsteady oblique freestream vortical modes is studied in direct numerical simulation of flow over a flat plate with an elliptic leading edge. The freestream is perturbed by three types of oblique Fourier modes, differing in the magnitude of the three vorticity components. The vortical modes excite steady boundary-layer streaks. The associated receptivity mechanism, described in detail, is quadratic in the forcing amplitude. Elliptic leading edges with two different aspect ratios are considered. We find that – and explain why – the streak amplitudes in nonlinear receptivity are largely unaffected by the leading-edge bluntness for the types of external disturbances studied. As linear receptivity is the predominant mechanism at low forcing frequencies, the nonlinear mechanism comes into play when high-frequency vortices are present in the freestream. Nonlinear receptivity is therefore expected to contribute to the excitation of boundary-layer streaks by freestream turbulence.

Keywords: nonlinear receptivity; freestream disturbances; elliptic leading edge; direct numerical simulation

1. Introduction

Receptivity is the initial stage of laminar-turbulent transition in boundary layers. The term denotes the mechanism by which freestream fluctuations or disturbances created by a rough aerodynamic surface are converted into boundary-layer instabilities. Here we present a direct numerical simulation (DNS) study of nonlinear receptivity to freestream vortical modes in boundary-layer flow over a flat plate with an elliptic leading edge.

Vortical freestream disturbances play a vital role in laminar-turbulent ‘bypass transition’ [1] of boundary layers. In wind tunnel experiments with freestream turbulence levels above 1% of the freestream speed, the dominant flow structures of pre-transitional flat-plate boundary layers are longitudinal streaks with alternating high and low streamwise velocity (see Figure 4 in [2]). Experiments reveal that quasi-steady counter-rotating streamwise freestream vortices are particularly effective in exciting these streaks [3]. The streamwise vortices constitute an ‘optimal disturbance’ [4], creating boundary-layer streaks with maximum transient amplification. The receptivity mechanism to these low-frequency vortices is linear in the amplitude of the freestream disturbance [5,6] and relies on the exchange of high- and low-speed fluid at the flanks of the vortices (termed ‘lift-up’ in [7]).

*Corresponding author. Email: lschrade@uottawa.ca

The role of the plate leading edge in linear receptivity to freestream vortical disturbances depends on the leading-edge geometry and the disturbance type. While the linear receptivity to steady streamwise vortices is barely affected by the bluntness of elliptic leading edges [6,8], the receptivity to steady vertical freestream vorticity is augmented by an increase of bluntness. This is caused by an intensification of tilting and stretching of the vertical vorticity lines at blunter leading edges, effecting a conversion of vertical into streamwise vorticity, as first explained by asymptotic analysis [9] and verified in experiments [10] and DNS [6]. Numerical simulations with freestream turbulence show that the enhancement of vortex stretching and tilting at blunter elliptic leading edges leads to an upstream shift of the transition location [11].

There also exists a nonlinear receptivity mechanism in boundary layers, driven by pairs of oblique freestream modes [5]. The interaction of two oblique waves was first analyzed in free shear layers [12]. The nonlinear receptivity mechanism to this type of disturbance, first discovered in channel flow [13], facilitates an effective laminar-turbulent transition route ('oblique-mode transition'), modelling many features of bypass transition in shear flows. Oblique-mode transition can also be realized in DNS [14,15] and wind-tunnel experiments [15] of boundary-layer flow over flat plates. Three steps are identified: the nonlinear generation of streamwise vortices by oblique modes, the formation of boundary-layer streaks by these vortices and the secondary streak instability, triggering the breakdown of the laminar streaks to turbulence. The streak generation through oblique modes can be reproduced by a weak nonlinear perturbation analysis [16]. Nonlinear receptivity to oblique waves is also observed in DNS of flat-plate boundary layers exposed to broadband freestream turbulence [17].

The study of nonlinear effects on streak formation in boundary layers is motivated by the observation that linear theories underpredict the streak amplitudes typically found in experiments with freestream turbulence. Moreover, nonlinearity affects the shape of the streaks and their secondary instability [18]. It is stated that 'nonlinear effects play an important role in the development of Klebanoff modes in many of the most important experiments' [19]. Further, 'this [nonlinear] effect increases with increasing downstream distance from the leading edge and possibly with increasing frequency', and 'the nonlinear effects may enter in a more or less quasi-steady manner' [19]. These statements are verified in the present paper, where the nonlinear boundary-layer response to freestream vortical modes with different frequencies is studied. We extend the earlier studies of nonlinear receptivity [5,14,16] by including the plate leading edge and vary its shape in order to identify bluntness effects on the receptivity. Since a wealth of different nonlinear disturbance interactions – symmetric and asymmetric – are possible in boundary layers exposed to freestream turbulence, we do not intend to present an exhaustive parametric study but limit our attention to symmetric interactions between pairs of oblique freestream modes. This paper follows a similar study of linear receptivity to vortical modes on the same geometry [6].

2. Flow configuration

We study the flow over a flat plate with a leading edge shaped as a modified super-ellipse (Figure 1). This contour features smoothness in wall curvature and hence a reduction of receptivity at the junction [20,21]. The super-ellipse is defined by

$$\left(\frac{y}{b}\right)^2 = 1 - \left(\frac{a-x}{a}\right)^p, \quad (1)$$

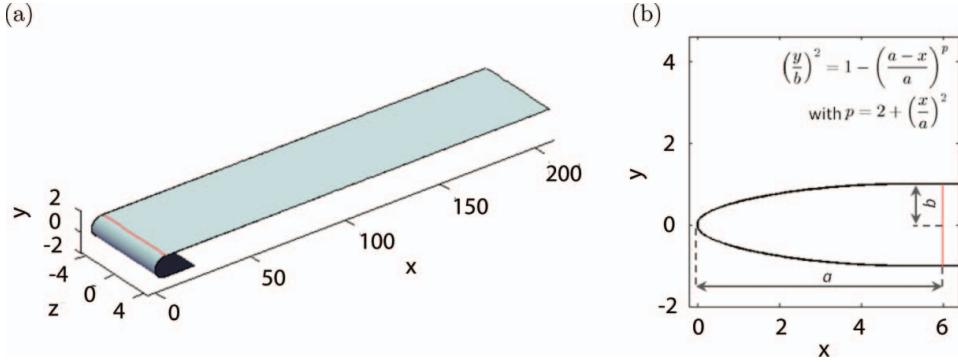


Figure 1. (a) Flat plate with elliptic leading edge ($AR = 6$). Lengths are normalized by the half-thickness b of the plate. The red line marks the leading-edge junction. (b) Modified super-ellipse (MSE), representing the leading-edge shape.

where the exponent p is

$$p = 2 + \left(\frac{x}{a}\right)^2. \quad (2)$$

We denote the streamwise, vertical and spanwise directions by x , y and z , and the respective velocities by U , V and W (baseflow) and u , v and w (disturbance). All lengths are scaled by the short semi-axis b of the leading edge. The long semi-axis, $a = AR \cdot b$, determines the bluntness of the nose, where AR stands for the aspect ratio of the leading edge. Here we consider $AR = 6$ and 20 . These values are also used in earlier numerical studies [6,21,22]. The reference speed is the freestream velocity U_∞ and the flow conditions are defined by the Reynolds number $Re = U_\infty b / \nu = 2400$. The outflow boundary is located at $x_{\text{out}} = 208.34b$ so that the outflow Reynolds number is $Re_{\text{out}} = U_\infty x_{\text{out}} / \nu = 5 \times 10^5$.

3. Numerical method

The simulations are carried out using the three-dimensional incompressible Navier–Stokes solver *Nek5000* [23] based on the spectral-element method (SEM) [24]. The SEM combines the high accuracy of global spectral methods with the geometrical flexibility of finite-element methods and is suitable for high-fidelity simulations of flow around bodies with surface curvature and leading edges. The physical domain is decomposed into spectral elements, upon which the solution is approximated by tensor products of Legendre polynomial Lagrangian interpolants. The expansion is written as

$$q^{(l)}(r, s, t) = \sum_{i=0}^N \sum_{j=0}^N \sum_{k=0}^N q_{ijk}^{(l)} h_i(r) h_j(s) h_k(t), \quad (3)$$

where q is a flow variable (e.g. the streamwise velocity), r , s and t are the local spatial coordinates of elements l , h_i , h_j , and h_k , respectively, are the i th, j th and k th order Lagrangian interpolants in the r -, s - and t -directions, q_{ijk} is the spectral coefficient and N is the highest polynomial degree included. The spatial allocation of the integration nodes is based on Gauss–Lobatto–Legendre (GLL) and Gauss–Legendre (GL) quadratures for the

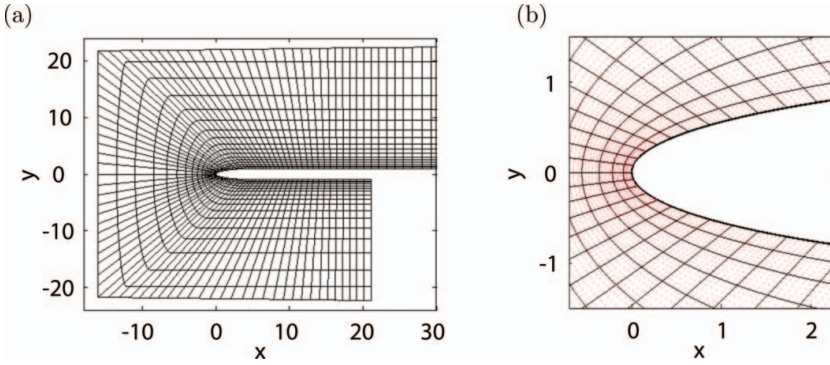


Figure 2. Spectral-element mesh for a plate with an elliptic leading edge ($AR = 6$). (a) Inflow region, and (b) close-up view of the leading edge. Spectral elements (black boxes) and GLL nodes (red dots).

velocity and pressure fields, respectively. Here we choose $N = 7$ for the velocity grid and $N = 5$ for the pressure grid ($\mathbb{P}_N\text{-}\mathbb{P}_{N-2}$ discretization; see [25]). This results in a staggered pressure grid with regard to the velocity grid, obviating the possibility of spurious pressure modes and rendering pressure boundary conditions unnecessary.

The computational mesh (Figure 2) is similar to the grids used in the preceding linear receptivity study [6]; however, the freestream boundary is streamline-shaped instead of straight. This is advantageous when freestream disturbances are convected downstream. For the three-dimensional simulations, 7650 elements are used, which amounts to nearly 2.8 million degrees of freedom. Dirichlet conditions for mean velocity at the inflow and freestream boundaries are generated from a potential-flow solution, including the streamline displacement by the boundary layer (see [6]). No-slip, no-stress and periodic conditions are applied at the wall, the outflow and the lateral boundaries, respectively.

3.1. Error estimator

The quality of the flow solution on a given computational mesh can be assessed by computing *a posteriori* error estimates. This is carried out here for two-dimensional simulations of the streamwise mean flow around the leading edge with $AR = 6$. The error estimator [26] is defined for each elemental direction separately (r and s here) as

$$\epsilon = \sqrt{\frac{q_N^2}{\frac{1}{2}(2N+1)} + \int_{N+1}^{\infty} \frac{q_n^2}{\frac{1}{2}(2n+1)} dn}, \quad (4)$$

where n is a placeholder for indices i and j in Equation (3). The quantity q_N is the highest order spectral coefficient of Equation (3) (i.e. $i = N$ or $j = N$), while the coefficients q_n for orders $N + 1$ and higher are estimated by an extrapolation of the spectrum (of the streamwise mean velocity here), using the exponential-decay relation $q_n = ce^{-\sigma n}$. The constant c and the decay rate σ are obtained through a least-squares best fit of the last four points ($N - 3, \dots, N$) of the resolved spectrum to an exponential decay.

The error estimator was originally developed to devise criteria for spectral-element mesh adaptation [27]. Here we use ϵ to investigate the error of the streamwise baseflow

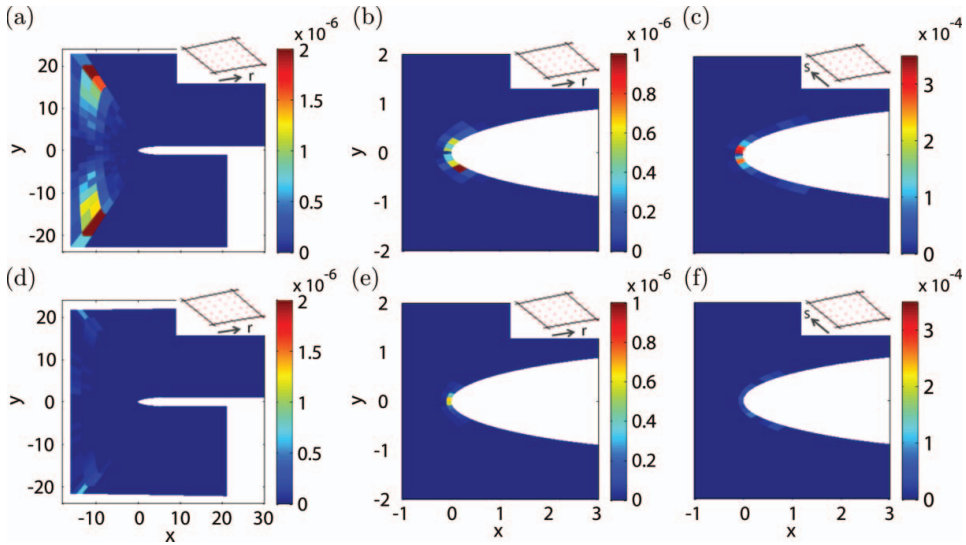


Figure 3. Error estimators of the streamwise baseflow around the plate with $AR = 6$ leading edge obtained with an initial SEM mesh ((a–c) from [6]) and an improved mesh (d–f). The error estimators are computed along two local elemental directions (cf. Equation (3)): r -direction (a–b, d–e) and s -direction (c, f). Errors in the inflow region (a, d) and near the leading edge are shown (b–c, e–f).

on a given mesh and improve the mesh manually as indicated by ϵ . Since ϵ estimates the one-dimensional spectrum of elemental approximation, we obtain $N + 1$ values of ϵ for each local direction per element. Averaging ϵ over these $N + 1$ values yields two error estimators per element for a two-dimensional simulation (one in the r - and another in the s -direction). The initial mesh (from [6]) produces an uneven error distribution in the inflow region (Figure 3(a)) and relatively large errors at the leading edge, especially in the s -direction (Figures 3(b) and (c)). This information is used to derive an improved numerical mesh (Figures 3(d)–(f)), where we only redistribute the elements while leaving the total number of elements and the spectral order unchanged. The major benefit of the improved mesh is a reduction of iterations in the pressure correction step and an ensuing acceleration of simulations by approximately 10%.

3.2. Freestream disturbance

Pairs of oblique vortical modes serve as a simple model of freestream turbulence. The vortical disturbances are prescribed as Fourier modes with spatial and temporal periodicity. The modal amplitude functions are those used in the earlier linear receptivity study [6], where three different types are considered (labelled ‘ ξ -’, ‘ η -’ and ‘ ζ -modes’). These differ in the dominant component of the vorticity vector (ξ , η , ζ). We point out that only two linearly independent vortical modes exist, the ξ - and the ζ -modes, whereas the third type (the η -mode) is not a physically independent solution [6]. It is nonetheless convenient to introduce all three modes because vortical modes with only one single vorticity component can easily be derived from ξ -, η - and ζ -modes. This is extensively utilized in the preceding study of linear receptivity to purely streamwise, vertical and spanwise freestream vorticity [6].

The inflow wave vector is $(\gamma, \beta) = (0.48, \pm 0.72)$, with γ and β being the vertical and spanwise wavenumbers. These values are consistent with those in the earlier study [6]; the

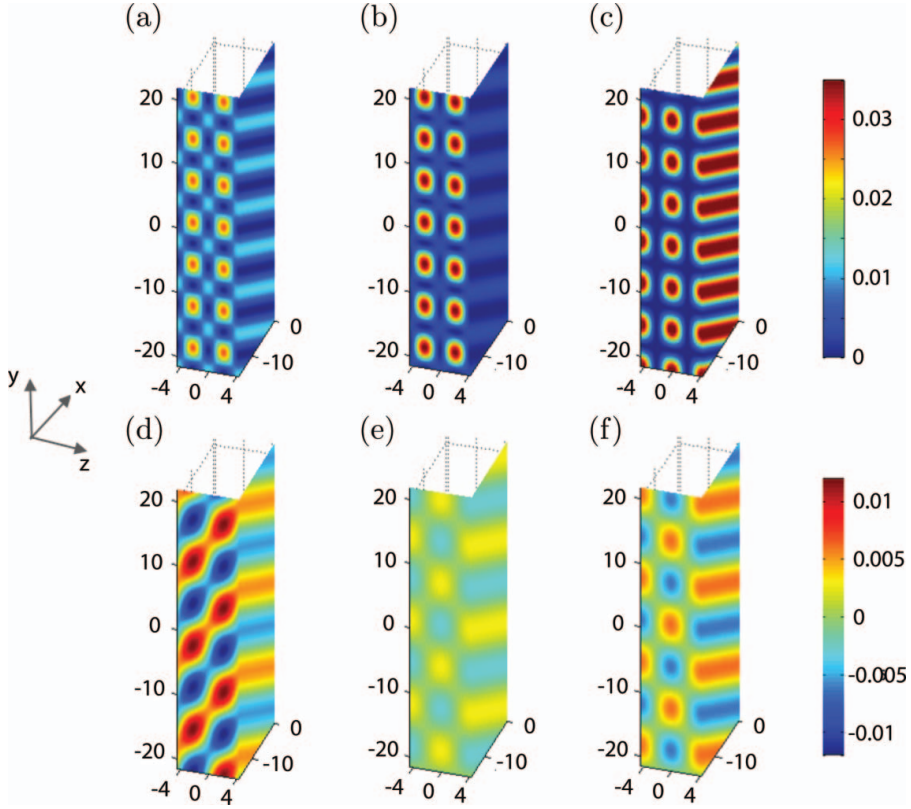


Figure 4. Inflow disturbance composed of pairs of oblique vortical modes (frequency $F = 96$, wave vector $(\gamma, \beta) = (0.48, \pm 0.72)$, amplitude $\varepsilon_{in} = 3.54 \times 10^{-3}$). Velocity magnitude of (a) ξ -modes, (b) η -modes and (c) ζ -modes. Streamwise vorticity of (d) ξ -modes, (e) η -modes and (f) ζ -modes.

only difference is that we also include the mode with spanwise wavenumber $\beta = -0.72$ and add it to the mode with $\beta = +0.72$. This produces a freestream vortical disturbance consisting of two oblique waves. The disturbance is scaled to obtain an amplitude of $\varepsilon_{in} = \sqrt{\bar{\mathbf{u}}_{in}^2}/2$. The bar denotes averaging over one wall-normal and spanwise wavelength in the inflow plane and over time, and \mathbf{u}_{in} is the disturbance-velocity vector at the computational inlet,

$$\mathbf{u}_{in} = \Re\{\hat{\mathbf{u}} e^{i(\gamma y \pm \beta z - \omega t)}\}, \quad (5)$$

with \Re denoting the real part. The quantity $\hat{\mathbf{u}} = (\hat{u}, \hat{v}, \hat{w})$ is the modal velocity coefficient and depends on the mode type (ξ -, η - or ζ -mode),

$$\xi\text{-mode:} \quad \hat{\mathbf{u}} = \frac{i}{\sqrt{\gamma^2 + \beta^2}} (0, \beta, -\gamma), \quad (6)$$

$$\eta\text{-mode:} \quad \hat{\mathbf{u}} = \frac{i}{\sqrt{\alpha^2 + \beta^2}} (-\beta, 0, \alpha), \quad (7)$$

$$\zeta\text{-mode: } \hat{\mathbf{u}} = \frac{i}{\sqrt{\alpha^2 + \gamma^2}} (\gamma, -\alpha, 0). \quad (8)$$

The derivation of Equations (6)–(8) is outlined in [6], where the vorticity amplitude functions for ξ -, η - and ζ -modes are also given. Invoking Taylor’s hypothesis, we replace the streamwise wavenumber α in Equations (6)–(8) by the angular frequency ω , which in turn is substituted by the frequency parameter, $F = [\omega/(U_\infty^2/\nu)] \times 10^6$. Figure 4 shows velocity magnitude and streamwise vorticity of inflow disturbances made up of pairs of oblique ξ -, η - and ζ -modes (frequency $F = 96$, wave vector $(\gamma, \beta) = (0.48, \pm 0.72)$, amplitude $\varepsilon_{\text{in}} = 3.54 \times 10^{-3}$). The ξ -modes feature the largest and the η -modes the smallest streamwise vorticity.

4. Results

4.1. Physical mechanism

The boundary-layer response to a pair of oblique ξ -modes with frequency $F = 96$ manifests itself mainly in the streamwise velocity (Figure 5(a)). In the upstream part of the boundary layer, the streamwise vortices in the freestream generate a disturbance with a short streamwise length scale (Figure 5(b)), where a patch of positive (negative) streamwise disturbance occurs on the downwash (upwash) side of vortices (‘lift-up effect’, Figure 6(a)). The velocity distribution of this disturbance is inverted farther downstream as the freestream vortices change the rotation direction (Figure 6(b)), indicating that the disturbance is unsteady and shares its streamwise wavelength with freestream modes. We also notice a second disturbance pattern near the wall with half the spanwise wavelength of freestream vortices, which is fixed in space in the downstream direction (Figures 6(b)–(d)) and takes the form of streamwise elongated streaks (Figure 5(b)). The steady nature of these streaks, their doubled spanwise wavenumber and their near-wall location suggest that they are not triggered directly by the fundamental freestream vortices but originate from a nonlinear process. This process creates weak counter-rotating longitudinal vortices

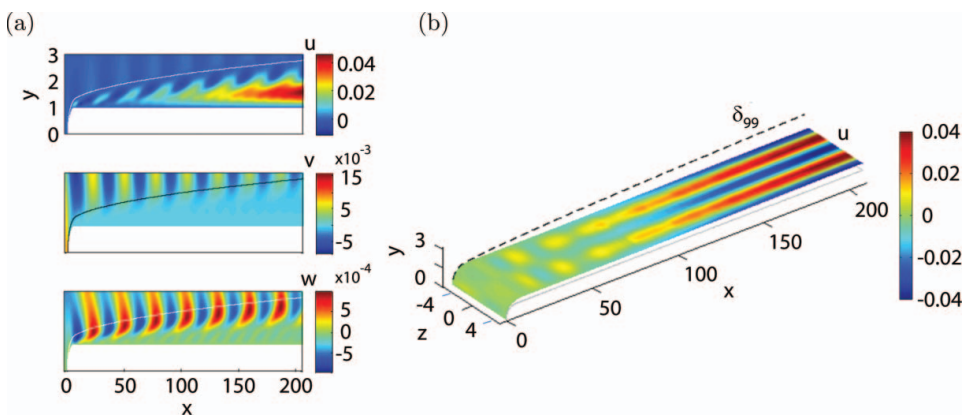


Figure 5. Boundary-layer response to a pair of oblique ξ -modes ($F = 96$, $(\gamma, \beta) = (0.48, \pm 0.72)$, $\varepsilon_{\text{in}} = 3.54 \times 10^{-3}$) for a plate with an elliptic leading edge ($AR = 6$). (a) x - y plane of streamwise, vertical and spanwise disturbance velocities ($z = 2.05$). Thin lines: δ_{99} . (b) Horizontal plane of streamwise disturbance at $y(\max_y(u_{\text{rms}}))$.

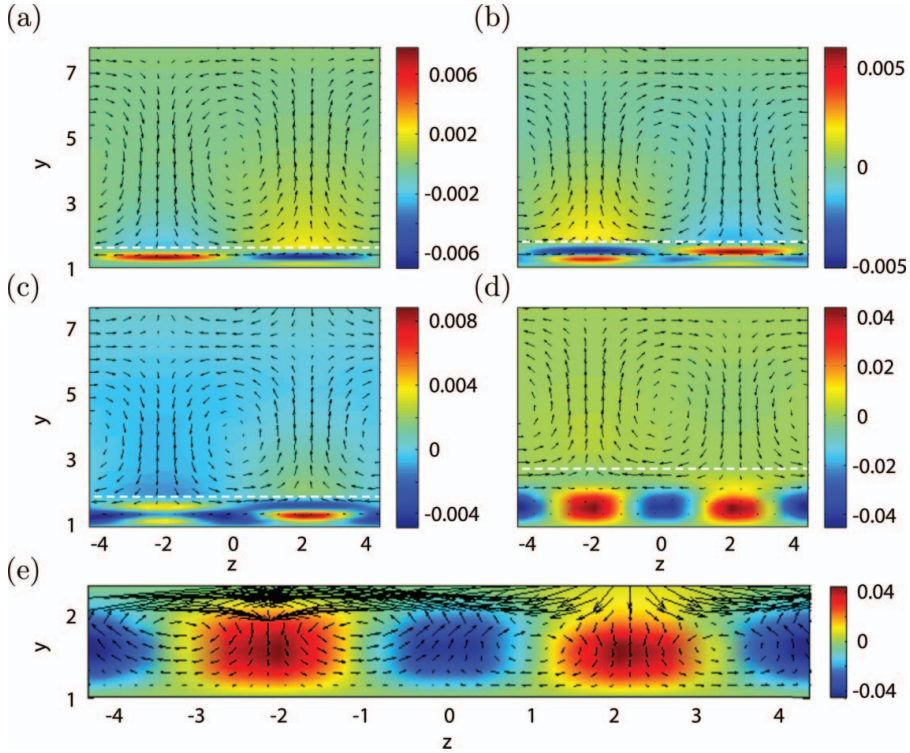


Figure 6. Cross-stream planes of streamwise velocity (colors) and wall-normal and spanwise velocities (vectors) at various downstream locations, showing the flow response to a pair of oblique ξ -modes ($F = 96$, $(\gamma, \beta) = (0.48, \pm 0.72)$, $\varepsilon_{\text{in}} = 3.54 \times 10^{-3}$) downstream of an elliptic leading edge ($AR = 6$). (a) $x = 20$; (b) 35; (c) 50; (d) 200. The white dashed line shows the local boundary-layer thickness (δ_{99}) . (e) Close-up view of (d), highlighting the details of the steady boundary-layer disturbance near the wall.

with half the fundamental spanwise wavelength, which penetrate the boundary layer more easily than the fundamental mode [16,28] and generate steady streaks by the lift-up effect (Figure 6(e)).

A temporal-spanwise Fourier decomposition of the total boundary-layer disturbance (u_{rms} curve in Figure 7(a)) confirms that the upstream disturbance is dominated by an unsteady short-scale mode with fundamental spanwise wavenumber, whereas the downstream disturbance evolution is mainly attributed to steady streaks with twice the fundamental wavenumber. This confirms that nonlinear effects appear ‘in a more or less quasi-steady manner’ [19]. The third and fourth most important contributions to the boundary-layer disturbance are the mean-flow modification $(0, 0)$ and the double-frequency mode $(2, \pm 2)$ (Figure 7(a)).

The nature of the boundary-layer receptivity is elucidated by considering boundary-layer forcing with two different amplitudes (ε_{in}) of the freestream disturbance (Figure 7(b)) and matching the evolution curves obtained for these two cases (Figure 7(c)). The unsteady fundamental mode amplitude is found to be linear in ε_{in} , whereas the steady streak amplitude scales as $\varepsilon_{\text{in}}^2$, suggesting a quadratic interaction of unsteady fundamental modes as being the source of the streaks. The amplitudes of modes $(0, 0)$ and $(2, \pm 2)$ are also proportional to $\varepsilon_{\text{in}}^2$ (not shown). Hence, the linear and nonlinear receptivity

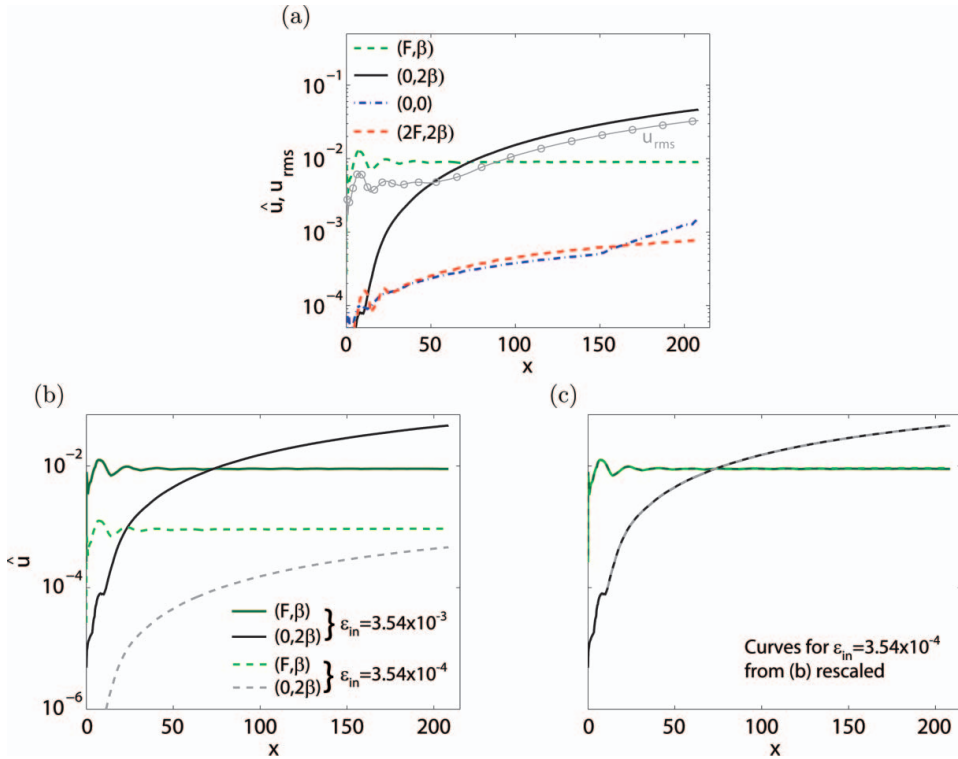


Figure 7. (a) Temporal-spanwise Fourier decomposition of the boundary-layer streamwise disturbance excited by a pair of oblique ξ -modes ($F = 96$, $(\gamma, \beta) = (0.48, \pm 0.72)$, $\varepsilon_{in} = 3.54 \times 10^{-3}$). Plate with $AR = 6$ leading edge. Besides the streamwise velocity amplitudes of different disturbance contributions (\hat{u}), the temporal-spanwise averaged streamwise rms of the total disturbance is shown (u_{rms}). All quantities are plotted at the wall distance of their maximum. (b) Comparison of the fundamental unsteady mode (F, β) and the steady and spanwise harmonic mode ($0, 2\beta$) for two forcing amplitudes: $\varepsilon_{in} = 3.54 \times 10^{-3}$ and 3.54×10^{-4} . (c) Rescaling of curves for $\varepsilon_{in} = 3.54 \times 10^{-4}$ from (b) so that they match the corresponding curves for $\varepsilon_{in} = 3.54 \times 10^{-3}$.

mechanisms act simultaneously in boundary layers subject to high-frequency freestream fluctuations.

When exposed to oblique η - and ζ -modes, the boundary layer develops steady disturbance streaks, too, but these streaks have lower amplitudes than those forced by ξ -modes (Figure 8). Since the ξ -modes feature a larger streamwise vorticity component than the η - and ζ -modes (Figure 4), we conclude that the boundary layer is nonlinearly most receptive to streamwise vorticity, as in the case of linear receptivity [6]. Interestingly, the $(0, 0)$ and $(2, \pm 2)$ components amplify less in an environment of oblique η -modes than in the presence of the other two mode types (Figure 8(a)).

4.2. Frequency effects

The effect of frequency is illuminated by comparing the standard case ($F = 96$) with two cases at a lower and a higher forcing frequency ($F = 16$ and 192), using oblique freestream waves of ξ -type. For $F = 16$, the disturbance (u_{rms} -curve) is made up mostly of the fundamental unsteady mode, whereas the steady double-spanwise wavenumber streak hardly contributes to u_{rms} (Figure 9(a)). The dominant receptivity mechanism of ξ -modes

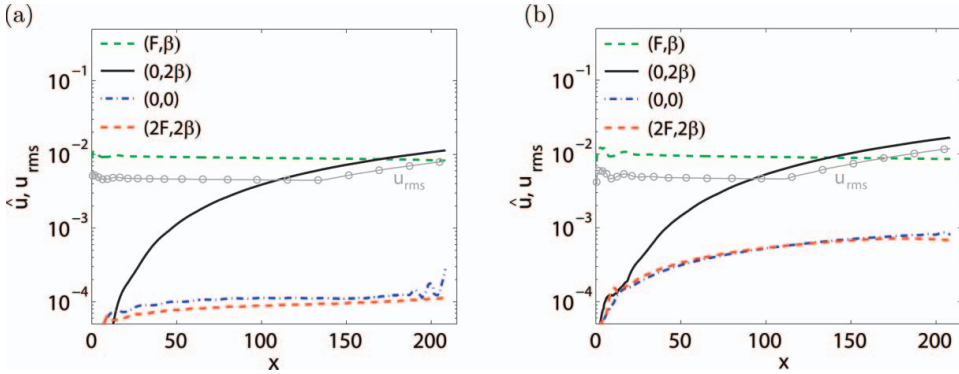


Figure 8. Temporal-spanwise Fourier decomposition of the boundary-layer streamwise disturbance excited by a pair of oblique (a) η -modes and (b) ζ -modes ($F = 96$, $(\gamma, \beta) = (0.48, \pm 0.72)$, $\varepsilon_{in} = 3.54 \times 10^{-3}$). The wall-normal maximum of each contribution is plotted. Plate with $AR = 6$ leading edge.

with $F = 16$ is thus linear and leads to the formation of slowly travelling streaks with finite length (see [29] for the relevance of these streaks in bypass transition). In contrast, the boundary-layer destabilization by oblique ξ -modes with $F = 192$ is almost entirely due to nonlinear receptivity, resulting in strong steady streaks (Figure 9(b)). Thus, the present simulations confirm the conjecture [19] that nonlinear effects on streak development may be more relevant at high frequencies.

4.3. Bluntness effects

So far, only the leading edge with $AR = 6$ has been used. In order to study leading-edge bluntness effects, we now also consider a more slender elliptic leading edge ($AR = 20$) and compare six different simulations (two leading edges times three mode types, ξ , η and ζ , at a frequency of $F = 96$). This confirms that the boundary layer is most receptive to ξ -modes

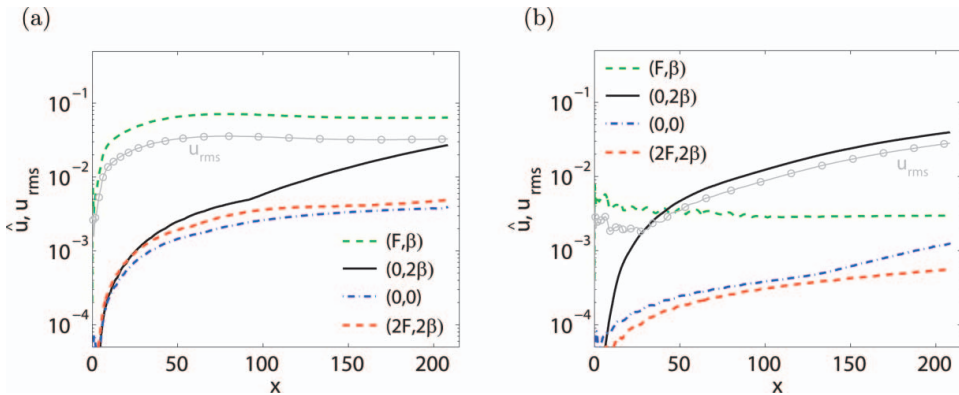


Figure 9. Temporal-spanwise Fourier decomposition of the boundary-layer streamwise disturbance excited by a pair of oblique ξ -modes ($(\gamma, \beta) = (0.48, \pm 0.72)$, $\varepsilon_{in} = 3.54 \times 10^{-3}$). The wall-normal maximum of each contribution is plotted. Plate with $AR = 6$ leading edge. Forcing frequency (a) $F = 16$ and (b) $F = 192$.

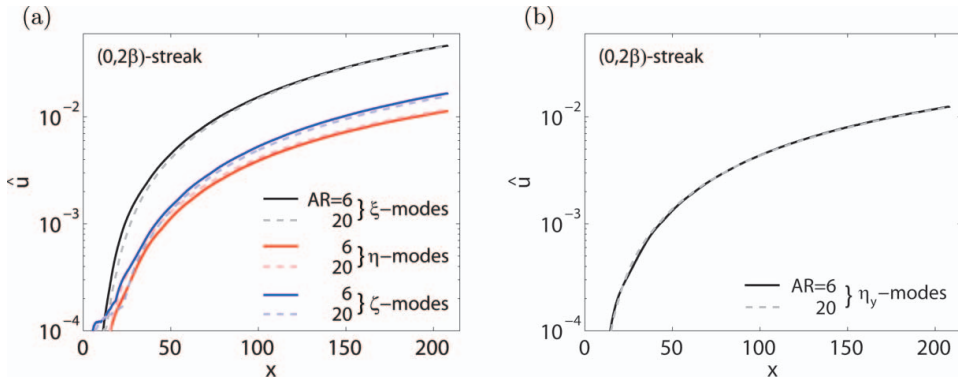


Figure 10. Comparison of two leading edges ($AR = 6$ and 20) in nonlinear receptivity to pairs of oblique modes. Wall-normal maximum of the streamwise amplitude of the $(0, 2\beta)$ -streak excited by (a) ξ -, η - and ζ -modes ($F = 96$, $(\gamma, \beta) = (0.48, \pm 0.72)$, $\varepsilon_{in} = 3.54 \times 10^{-3}$) and (b) η_y -modes (purely vertical vorticity; $\gamma = 0$, $F = 96$, $\beta = \pm 0.72$, $\varepsilon_{in} = 3.38 \times 10^{-3}$).

and least receptive to η -modes (Figure 10(a)). Most notably, the nonlinear receptivity to all three types of freestream vorticity is largely unaffected by the bluntness of the elliptic leading edge.

Linear boundary-layer receptivity is known to become dependent on the leading-edge aspect ratio under certain freestream disturbance conditions: If triggered by steady freestream modes with vertical vorticity only, the boundary-layer streaks intensify in the presence of a blunter elliptic leading edge [6]. The vertical-vorticity modes (denoted as ‘ η_y -modes’ in [6]) are constructed by setting the vertical wavenumber γ of η -modes to zero. Key to the receptivity mechanism is the conversion of vertical vorticity into streamwise vorticity by tilting and stretching of vorticity lines at the leading edge [9] – processes that are more effective at blunter leading edges (see also Figure 15 in [6]).

In order to clarify whether a similar dependence on bluntness also exists in nonlinear receptivity, we use a pair of unsteady η_y -modes ($F = 96$) here, invoking the quadratic receptivity mechanism. However, changing the leading-edge shape does not alter the amplitude of steady streaks (Figure 10(b)). This suggests that the nonlinear receptivity process to the unsteady η_y -modes is fundamentally different from the linear mechanism to the steady η_y -modes. In the present scenario, the oncoming vertical vortex columns (Figure 11, plane 1) directly enforce a streamwise disturbance at the nose of the plate, which evolves as a nonmodal instability (plane 2). The lift-up mechanism, driven by vertical vortices here, is most effective in the close vicinity of the nose. Most notably, we do not observe considerable streamwise vortices farther downstream (plane 3), i.e. a conversion of vertical into streamwise vorticity near the boundary-layer edge by vortex tilting and stretching does not significantly take place. Instead, the near-wall streamwise vortices (not shown in Figure 11) forming the downstream dominant steady streaks (plane 4) are created through quadratic interactions of upstream unsteady disturbances. This process is independent of leading edge and thus insensitive to nose bluntness.

4.4. Receptivity coefficients

The different cases of nonlinear receptivity studied are summarized by compiling the associated receptivity coefficients in Table 1 (for $AR = 6$ only). These relate the amplitude

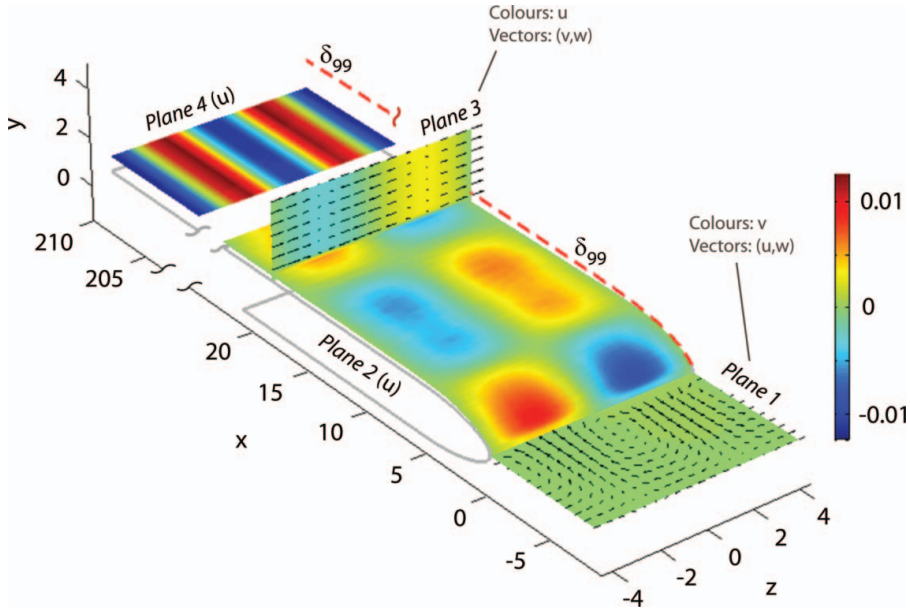


Figure 11. Details at the leading edge ($AR = 6$) of the nonlinear receptivity to η_y -modes (purely vertical vorticity; $\gamma = 0$, $F = 96$, $\beta = \pm 0.72$, $\varepsilon_{in} = 3.38 \times 10^{-3}$). Plane 4 is located much farther downstream than apparent in the figure as large parts of the x -axis are cut out to save space.

of the boundary-layer instability to that of the triggering disturbance,

$$C_{nl} = \frac{A_{str}}{\varepsilon_{le}^2}, \quad (9)$$

thus measuring the efficiency of the receptivity mechanism. A_{str} is the streak amplitude, defined here by the streamwise velocity amplitude \hat{u} of the steady streak. We extract A_{str} far downstream at $x = 208$ ($Re_x = 5 \times 10^5$), where the $(0, 2\beta)$ -streak is easily identifiable in all cases. The freestream disturbance level is evaluated at the leading edge, where ε_{le} is defined similar to ε_{in} (see Section 3.2) but computed on the z - y plane at the nose ($x = 0$). This reflects that the receptivity mechanism is initiated at the leading edge. Using the square of ε_{le} in Equation (9) accounts for the quadratic nature of the receptivity mechanism. It turns out in all cases that the freestream disturbance decays very little on travelling from the inflow plane to the leading edge ($\varepsilon_{le} \approx \varepsilon_{in}$) so that we use ε_{in} to evaluate Equation (9).

Table 1. Receptivity coefficients (C_{nl} , Equation (9)) for nonlinear receptivity to pairs of oblique ξ -, η - and ζ -modes with wavenumber vector $(\gamma, \beta) = (0.48, \pm 0.72)$, and η_y -modes with $(\gamma, \beta) = (0, \pm 0.72)$ and frequency $F = 96$. Two additional frequencies ($F = 16$ and 192) are considered in the case of ξ -modes. The leading-edge $AR = 6$ is used.

	ξ -modes	η -modes	ζ -modes	η_y -modes
$F = 16$	2170			
$F = 96$	3729	911	1336	1098
$F = 192$	3170			

The highest receptivity coefficients are obtained for the oblique ξ -modes, thanks to their large streamwise vorticity (cf. Figure 4). The steady boundary-layer streaks are most receptive to ξ -modes with $F = 96$, attaining a more than four times higher amplitude than in the presence of η -modes with $F = 96$. Even at the lowest frequency ($F = 16$), for which the linear receptivity mechanism takes precedence over the nonlinear mechanism (see Figure 9(a)), the ξ -modes still produce stronger steady streaks than the η - and ζ -modes with $F = 96$.

4.5. Nonlinear versus linear receptivity

In order to assess the relevance of the nonlinear receptivity mechanism relative to the linear mechanism, we compare the downstream evolution of two steady boundary-layer streaks with the same spanwise wavenumber ($\beta = 1.44$) but different origin: the first streak is excited by a pair of oblique ξ -modes with wavenumber $\beta = \pm 0.72$ and frequency $F = 96$ (nonlinear receptivity), whereas the second streak is triggered by a single ξ -mode with $\beta = 1.44$ and $F = 0$ (linear receptivity). The amplitudes of these two streaks are written as

$$A_{\text{str,nln}}(x) = C_{\text{nln}}(x) \varepsilon_{\text{le,nln}}^2, \tag{10}$$

$$A_{\text{str,lin}}(x) = C_{\text{lin}}(x) \varepsilon_{\text{le,lin}}, \tag{11}$$

where $\varepsilon_{\text{le,nln}}$ and $\varepsilon_{\text{le,lin}}$ are the forcing amplitudes of nonlinear and linear receptivity mechanisms, extracted at the leading edge ($x = 0$), and C_{nln} and C_{lin} are local nonlinear and linear receptivity coefficients. Since $A_{\text{str,nln}}$ and $A_{\text{str,lin}}$ scale differently with amplitude ε of freestream disturbances, the relative importance of nonlinear and linear receptivity changes with ε . For the example of $\varepsilon_{\text{le,nln}} = \varepsilon_{\text{le,lin}} = 3.54 \times 10^{-3}$, the linear receptivity mechanism produces a significantly larger streak amplitude than the nonlinear mechanism (Figure 12(a)). We also notice that the two streaks amplify at different streamwise rates since these are generated in different regions of the boundary layer (under different flow conditions): the linear receptivity mechanism is initiated directly at the leading edge, where

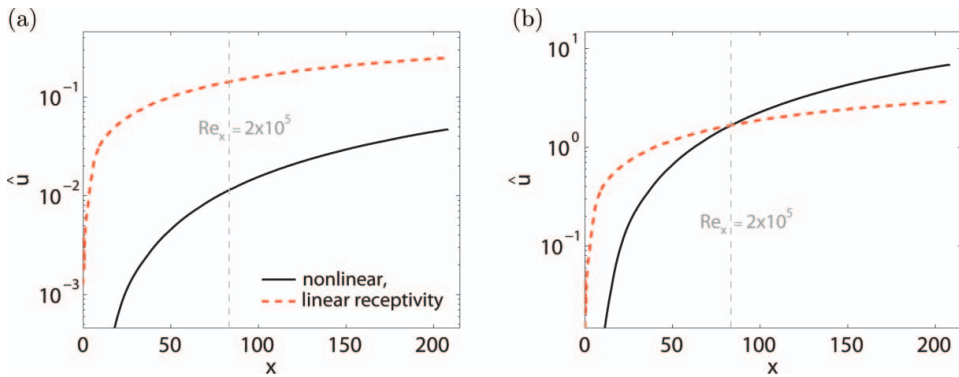


Figure 12. Comparison of two steady streaks ($\beta = 1.44$) with different origins: excitation by (i) a pair of unsteady oblique ξ -modes (nonlinear receptivity), and (ii) a single steady ξ -mode (linear receptivity) with the same amplitude: (a) $\varepsilon = 3.54 \times 10^{-3}$, and (b) $\varepsilon = 4.30 \times 10^{-2}$. The wall-normal maximum of the streamwise disturbance amplitude is shown. In (b), the streak amplitudes become identical at $Re_x = 2 \times 10^5$.

it produces significant transient growth, while the nonlinear process involves several stages, thus acting over a longer stretch of the boundary layer.

Since nonlinear receptivity becomes more competitive with increasing ε , a threshold amplitude $\varepsilon_{\text{thresh}}(x)$ exists, at which the nonlinearly excited streak becomes as strong at a certain streamwise location x as the streak due to linear receptivity. This threshold is identified by equating Equations (10) and (11) as $\varepsilon_{\text{thresh}}(x) = C_{\text{lin}}(x)/C_{\text{nlm}}(x)$. For $x = 83$ ($Re_x = 2 \times 10^5$), we read off from Figure 12(a) streak amplitudes of $A_{\text{str,nln}} = 0.0113$ and $A_{\text{str,lin}} = 0.1370$. This yields $C_{\text{nlm}} = 904.45$ and $C_{\text{lin}} = 38.73$ so that $\varepsilon_{\text{thresh}} = 0.043$. Such high-level free-stream disturbances would create energetic streaks (Figure 12(b)) with amplitudes far above typical thresholds of incipient secondary streak instability and breakdown (see [30]), i.e. these streaks are not realizable. This suggests that the linear receptivity mechanism is more relevant in typical vortical disturbance environments than the nonlinear mechanism. Since $\varepsilon_{\text{thresh}}$ drops with increasing distance from the leading edge (e.g. $\varepsilon_{\text{thresh}} = 0.018$ at $x = 208$ or $Re_x = 5 \times 10^5$), the nonlinear receptivity mechanism becomes more competitive farther downstream. Moreover, $\varepsilon_{\text{thresh}}$ depends on the frequency of the oblique vortical modes triggering the nonlinear streak.

5. Summary and discussion

This paper reports a study of nonlinear (quadratic) boundary-layer receptivity to unsteady freestream vorticity. To this end, we perform DNS of flow past an elliptic leading edge, considering pairs of unsteady oblique vortical freestream modes. The present work extends previous investigations of nonlinear receptivity to oblique modes [5, 14, 16] by including the plate leading edge and is a follow-up of an earlier study on linear receptivity [6]. The spectral-element method used proves particularly efficient when combined with an error-estimator-based mesh improvement to treat the leading-edge region.

The focus of this paper is on the physical processes and the role of elliptic leading edges in nonlinear boundary-layer receptivity of steady streaks to high-frequency oblique freestream modes. The receptivity mechanism, earlier reported for flat-plate boundary layers without leading edges [5, 14, 16], involves the following stages: (1) quadratic interactions of the fundamental unsteady perturbation, creating weak steady streamwise vortices with half the fundamental spanwise wavelength; and (2) the linear lift-up process of these vortices, forming steady streamwise streaks with significantly larger amplitudes than the upstream fundamental disturbance (cf. Figure 6). The steady vortex-streak system obtained amplifies through the transient-growth mechanism of the shear layer and may further be energized along the entire boundary-layer edge through continuous forcing by weak nonlinear streamwise freestream vortices [31]. The quadratic receptivity mechanism is most effective if the frequency of the freestream vortices is high. The largest streak amplitudes are obtained when the freestream modes bear mainly streamwise vorticity, as in linear receptivity [6].

The streak intensity is largely unaffected by the bluntness of the elliptic leading edge for the range of aspect ratios considered, irrespective of the dominant vorticity component of the freestream disturbance. This is contrary to linear receptivity, where blunt leading edges enhance the receptivity to vertical freestream vorticity: The leading edge distorts the oncoming vertical vorticity and converts it into streamwise vorticity through vortex stretching and tilting [9] – processes that are intensified by blunter leading edges [6]. In the present nonlinear receptivity mechanism, the streamwise vortices required for streak excitation are not created by vortex stretching and tilting at the leading edge, but these emerge farther downstream through quadratic disturbance interactions. These interactions are

independent of the leading-edge bluntness. The leading edge plays nonetheless an important role in nonlinear receptivity, because the impingement and boundary-layer penetration of freestream disturbances happen at the nose of the plate (cf. Figure 11).

Although linear receptivity appears to be more effective, nonlinear receptivity is shown to come into play when high-frequency disturbances are present in the freestream. Direct numerical simulation studies of boundary layers exposed to broadband freestream turbulence [17] reveal that the nonlinear receptivity mechanism to oblique freestream waves is active if the higher frequency range of the turbulent spectrum contains sufficient energy. In such disturbance environments, the boundary-layer streaks are created and energized by the linear and the nonlinear receptivity mechanisms simultaneously, where the nonlinear mechanism sets in farther downstream than the linear mechanism. This may at least in part explain the discrepancy observed downstream between experimentally measured streak amplitudes and those predicted by linear receptivity and instability theories.

Acknowledgements

The authors gratefully acknowledge funding by Natural Sciences and Engineering Research Council of Canada (NSERC) and The Swedish Research Council (VR). Computer time by SNIC/NSC (National Supercomputer Centre, Linköpings universitet) is acknowledged.

References

- [1] M.V. Morkovin, *On the many faces of transition*, in *Viscous Drag Reduction*, C.S. Wells, ed., Plenum, New York, 1969, pp. 1–31.
- [2] M. Matsubara and P.H. Alfredsson, *Disturbance growth in boundary layers subjected to free-stream turbulence*, *J. Fluid Mech.* 430 (2001), pp. 149–168.
- [3] F.P. Bertolotti and J. Kendall, *Response of the Blasius boundary layer to controlled free-stream vortices of axial form*, AIAA Paper 97-2018 (1997).
- [4] P. Andersson, M. Berggren, and D.S. Henningson, *Optimal disturbances and bypass transition in boundary layers*, *Phys. Fluids* 11(1) (1999), pp. 134–150.
- [5] S. Berlin and D.S. Henningson, *A nonlinear mechanism for receptivity of free-stream disturbances*, *Phys. Fluids* 11(12) (1999), pp. 3749–3760.
- [6] L.U. Schrader, L. Brandt, C. Mavriplis, and D.S. Henningson, *Receptivity to free-stream vorticity of flow past a flat plate with elliptic leading edge*, *J. Fluid Mech.* 653 (2010), pp. 245–271.
- [7] M.T. Landahl, *Wave breakdown and turbulence*, *SIAM J. Appl. Math.* 28(4) (1975), pp. 735–756.
- [8] J.M. Kendall, *Studies on laminar boundary-layer receptivity to freestream turbulence near a leading edge*, in *Boundary Layer Stability and Transition to Turbulence; Proceedings of the Symposium of 1st ASME and JSME Joint Fluids Engineering Conference, Portland, OR*, ASME, New York, 1991, pp. 23–30.
- [9] M.E. Goldstein and D.W. Wundrow, *On the environmental realizability of algebraically growing disturbances and their relation to Klebanoff modes*, *Theor. Comput. Fluid Dyn.* 10 (1998), pp. 171–186.
- [10] M.N. Kogan, V.G. Shumilkin, M.V. Ustinov, and S.V. Zhigulev, *Response of boundary layer flow to vortices normal to the leading edge*, *Eur. J. Mech. B – Fluids* 20 (2001), pp. 813–820.
- [11] S. Nagarajan, S.K. Lele, and J.H. Ferziger, *Leading-edge effects in bypass transition*, *J. Fluid Mech.* 572 (2007), pp. 471–504.
- [12] M.E. Goldstein and S.W. Choi, *Nonlinear evolution of interacting oblique waves on two-dimensional shear layers*, *J. Fluid Mech.* 207 (1989), pp. 97–120.
- [13] P.J. Schmid and D.S. Henningson, *A new mechanism for rapid transition involving a pair of oblique waves*, *Phys. Fluids A* 4(9) (1992), pp. 1986–1989.
- [14] S. Berlin, A. Lundbladh, and D. Henningson, *Spatial simulations of oblique transition in a boundary layer*, *Phys. Fluids* 6(6) (1994), pp. 1949–1951.

- [15] S. Berlin, M. Wiegel, and D.S. Henningson, *Numerical and experimental investigations of oblique boundary layer transition*, J. Fluid Mech. 393 (1999), pp. 23–57.
- [16] L. Brandt, D.S. Henningson, and D. Ponziani, *Weakly non-linear analysis of boundary layer receptivity to free-stream disturbances*, Phys. Fluids 14 (2002), pp. 1426–1441.
- [17] L. Brandt, P. Schlatter, and D.S. Henningson, *Transition in boundary layers subject to free-stream turbulence*, J. Fluid Mech. 517 (2004), pp. 167–198.
- [18] P. Ricco, J. Luo, and X. Wu, *Evolution and instability of unsteady nonlinear streaks generated by free-stream vortical disturbances*, J. Fluid Mech. 677 (2011), pp. 1–38.
- [19] S.J. Leib, D.W. Wundrow, and M.E. Goldstein, *Effect of free-stream turbulence and other vortical disturbances on a laminar boundary layer*, J. Fluid Mech. 380 (1999), pp. 169–203.
- [20] M.E. Goldstein and L.S. Hultgren, *Boundary-layer receptivity to long-wave free-stream disturbances*, Annu. Rev. Fluid Mech. 21 (1989), pp. 137–166.
- [21] N. Lin, H. Reed, and W. Saric, *Effect of leading edge geometry on boundary-layer receptivity to freestream sound*, in *Instability, Transition and Turbulence*, M. Hussaini, A. Kumar, and C. Streett, eds., Springer, New York, 1992, pp. 10–29.
- [22] J.B.V. Wanderley and T.C. Corke, *Boundary layer receptivity to free-stream sound on elliptic leading edges of flat plates*, J. Fluid Mech. 429 (2001), pp. 1–21.
- [23] P. Fischer, J. Kruse, J. Mullen, H. Tufo, J. Lottes, and S. Kerkemeier, *NEK5000 – Open source spectral element CFD solver* (2008). Available as of May, 2012, at <http://nek5000.mcs.anl.gov/index.php/MainPage>.
- [24] A.T. Patera, *A spectral element method for fluid dynamics: Laminar flow in a channel expansion*, J. Comp. Phys. 54 (1984), pp. 468–488.
- [25] Y. Maday and A.T. Patera, *Spectral element methods for the Navier-Stokes equations*, in *State of the Art Surveys in Computational Mechanics*, A.K. Noor, ed., ASME, New York, 1989, pp. 71–143.
- [26] C. Mavriplis, *A posteriori error estimators for adaptive spectral element techniques*, in *Notes on Numerical Fluid Mechanics*, vol. 29, P. Wesseling, ed., Vieweg Braunschweig, Berlin, Germany, 1990, pp. 333–342.
- [27] C. Mavriplis, *Adaptive mesh strategies for the spectral element method*, Comput. Methods Appl. Mech. Eng. 116 (1994), pp. 77–86.
- [28] R.G. Jacobs and P.A. Durbin, *Shear sheltering and continuous spectrum of the Orr-Sommerfeld equation*, Phys. Fluids 10(8) (1998), pp. 2006–2011.
- [29] L. Brandt and H.C. deLange, *Streak interactions and breakdown in boundary layer flows*, Phys. Fluids 20 (2008), pp. 1–16.
- [30] P. Andersson, L. Brandt, A. Bottaro, and D.S. Henningson, *On the breakdown of boundary layer streaks*, J. Fluid Mech. 428 (2001), pp. 29–60.
- [31] K.J.A. Westin, A.A. Bakchinov, V.V. Kozlov, and P.H. Alfredsson, *Experiments on localized disturbances in a flat plate boundary layer. Part 1. The receptivity and evolution of a localized free stream disturbance*, Eur. J. Mech. B – Fluids 17(6) (1998), pp. 823–846.